Materials Horizons

ROYAL SOCIETY OF CHEMISTRY

COMMUNICATION

View Article Online
View Journal | View Issue

Cite this: *Mater. Horiz.*, 2023, 10, 2516

Received 1st March 2023,
Accepted 9th April 2023

DOI: 10.1039/d3mh00310h

rsc.li/materials-horizons

Direct ink writing of PEDOT eutectogels as substrate-free dry electrodes for electromyography†

Ana Aguzin, ‡[a] Antonio Dominguez-Alfaro,‡[bc] Miryam Criado-Gonzalez,[b] Santiago Velasco-Bosom,[c] Matías L. Picchio, [ab] Nerea Casado, [bd] Eleni Mitoudi-Vagourdi,[c] Roque J. Minari, [a] George G. Malliaras*[c] and David Mecerreyes *[bd]

Deep Eutectic Solvents (DES) are a new class of ionic conductive compounds attracting significant attention as greener alternatives to costly ionic liquids. Herein, we developed novel mixed ionic-electronic conducting materials by simple mixing of poly(3,4-ethylenedioxythiophene)/poly(styrenesulfonate) (PEDOT:PSS) and various DES as additives. The DES addition induces the supramolecular assembly and gelification of PEDOT:PSS forming eutectogels triggered by extensive hydrogen bonding and charge stabilization. The eutectogels feature boosts the mixed ionic–electronic conductivity of PEDOT:PSS up to 368 S cm^{-1}, unveiling great potential as flexible bioelectronics. All the PEDOT:PSS/DES gels showed shear-thinning behavior and viscosity values ranging from 100 to 1000 Pa s. The eutectogels show good injectability with almost instantaneous elastic recovery, making them ideal materials for direct ink writing (DIW). As proof of that, PEDOT:PSS/DES (choline chloride:lactic acid) was 3D printed in different patterns, annealed at high temperature, and assembled into adhesive electrodes. This way tattoos-like electrodes, denoted as Eutecta2 were fabricated and placed *in vivo* on the forearm and the thumb of human volunteers for electromyography measurements. Eutecta2 hexagonal patterns showed excellent conformability, and their signal-to-noise ratio (SNR) was higher than Ag/AgCl commercial electrodes for thumb motion measurements. Furthermore, forearm motion was measured after 14 days with similar values of SNR, demonstrating long-term stability and reusability. All in all, our findings revealed that DES could be used as inexpensive and safe additives to direct the self-assembly of PEDOT:PSS into supramolecular eutectogels inks for flexible bioelectronics.

New concepts

In this work, we demonstrate the concept of mixed ionic electronic conductive materials by the combination of PEDOT:PSS and deep eutectic solvents (DESs). The extensive hydrogen bonding and charge stabilization of the DESs greatly enhances the PEDOT:PSS electrical and ionic conductivity up to 450 S cm^{-1} and 0.16 S cm^{-1}, respectively. Unlike previous systems based on PEDOT:PSS/ionic-liquids, PEDOT:PSS/DESs are cost-effective, easy to make, have similar conductivity values and are more biocompatible. Furthermore, the PEDOT:PSS DES show shear-thinning properties which allows the direct printing of electrodes for electrophysiology, called eutectic-tattoos (Eutecta2). The obtained Eutecta2 electrodes are self-standing, stable after drying, and reusable, as well as 3D printable in custom shapes. They were placed *in vivo* on the forearm and thumb of human volunteers for electromyography measurements, demonstrating conformability-dependent to shape and a better signal-to-noise ratio (SNR) than commercial electrodes. In conclusion, PEDOT:PSS/DESs are a new class of mixed ionic–electronic materials that could play a crucial role in the field of flexible bioelectronics, offering unique advantages over traditional materials reported in the literature.

Introduction

Wearable health monitoring devices have become increasingly prevalent among consumers and healthcare diagnoses in the last few years, becoming a powerful tool in preventing and detecting diseases at early stages.[1] Among various bio-signals, electrical recordings of bio-potentials such as electrocardiography (ECG), electromyography (EMG), and electroencephalography (EEG) are key in the monitoring and diagnosis process.[2]

Up to now, wet Ag/AgCl gel electrodes have been the most employed in real scenarios due to their relatively low cost and

[a] *Instituto de Desarrollo Tecnológico para la Industria Química (INTEC), CONICET, Güemes 3450, Santa Fe 3000, Argentina*
[b] *POLYMAT, University of the Basque Country UPV/EHU, Avenida Tolosa 72, Donostia-San Sebastián, Gipuzkoa 20018, Spain. E-mail: david.mecerreyes@ehu.es*
[c] *Electrical Engineering Division, Department of Engineering, University of Cambridge, 9 JJ Thomson Ave, Cambridge, CB3 0FA, UK. E-mail: gm603@cam.ac.uk*
[d] *IKERBASQUE, Basque Foundation for Science, 48009, Bilbao, Spain*

† Electronic supplementary information (ESI) available. See DOI: https://doi.org/10.1039/d3mh00310h

‡ These authors contributed equally to this work.

high sensitivity. Regrettably, these electrodes may cause skin irritation and deteriorate after volatilization of the liquid inside the gel electrolyte, rendering them inappropriate for long-term and wearable monitoring. In contrast, dry electrodes are a promising alternative to overcome stability and contact issues. In particular, dry tattoos made of conducting materials (e-tattoos) that are biocompatible, conformable, and self-adhesive to the skin represent a potential solution. In this vein, poly(3,4-ethylenedioxitiophene) doped with polystyrene sulfonate (PEDOT:PSS) is the gold standard material for electrical bio-recording.[3,4] The strength of this organic conductor resides in its mixed conductivity, being able to conduct electrons and ionic charges, enhancing conversion of ionic signals into electronic ones. Nevertheless, PEDOT:PSS is neither stretchable nor adhesive to the skin and possesses a bulk electrical conductivity that is not wholly satisfactory when micrometer-size materials are required. Moreover, PEDOT:PSS is only processable by spin-coating methods, limiting electrode geometry and self-portability. In this regard, inkjet printing that processes the material in 2D is the only alternative that has been used to manufacture e-tattoos.[5,6] Poly(vinyl alcohol) and dimethyl sulfoxide have been applied as dopants to improve the conductivity and flexibility of PEDOT:PSS, reporting similar interface impedance to Ag/AgCl electrodes when the electrode was wet.[7] In recent works, PEDOT:PSS without any other additive was inkjet printed on tattoo paper and skin-transferred, measuring ECG and EMG with nanometer-thick electrodes but exhibiting impedance values a few orders of magnitude higher than commercial ones. Despite the delicate material and easy transfer method, impedance in dried state is detrimental to addressing long-term recording and mechanical or time stability challenges.[8–10]

One of the solutions to render PEDOT:PSS more suitable for these applications is the incorporation of ionically conductive additives,[11] such as ionic liquids (ILs). When mixed with PEDOT:PSS, ILs act as effective secondary dopants, enhancing the global conductivity by more than 1000-fold. Besides the conductivity enhancement, ILs act as plasticizers and make PEDOT:PSS incredibly stretchable, with deformations surpassing 100%.[12] Unfortunately, the ILs that show higher conductivity enhancement possess high toxicity and poor biodegradability, which is prohibitive for applications where intimate contact with the skin is required.[13,14] In this regard, some of us recently described some skin-friendly ILs composed of cholinium-carboxylate for bioelectronics.[15]

In the next generation of additives, deep eutectic solvents (DES) have started to unseat the role of ILs. DES are mixtures of pure compounds, commonly called hydrogen bond acceptors (HBA) and hydrogen bond donors (HBD), for which the eutectic point temperature is significantly lower than that of an ideal liquid mixture.[16–18] DES benefit from a broad liquid range, easy and green synthesis, which avoids solvent and purification steps, and possess low toxicity and cost because their components are often renewable resources.[19,20] DES have been mostly combined with PEDOT:PSS electrochemically, acting as a supporting electrolyte during the polymerization and therefore doping PEDOT,[21] and only a few works have explored DES for PEDOT post-treatment.[22–24] Very recently, DES have been used to develop the first mixed ionic–electronic eutectogel for electrocardiogram (ECG) and electromyogram (EMG) recordings. The material was composed of glyceline (choline chloride: glycerol, ChCl : Gly 1 : 2 mol ratio), PEDOT: lignin sulfonate, and gelatin. The eutectogel improved the processability of PEDOT material, rendering it excellent for 3D printing by direct ink-writing.[25]

In this work, we described innovative supramolecular eutectogels based on the combination of PEDOT:PSS with a series of DES composed of ChCl as a typical HBA and various HBD from aliphatic polyols, organic acids to aromatic compounds *i.e.* ChCl : Gly (1 : 2), ChCl : 1,3-propanediol (PDO) (1 : 2), ChCl : lactic acid (LAC) (1 : 2), ChCl:pyrogallol (PY) (1 : 1) and ChCl : *p*-toluenesulfonic acid (PTSA) (1 : 1). Supramolecular eutectogels were only obtained at PEDOT:PSS/DES ratios higher than 30 wt% due to charges equilibrium. We studied the impact of the chemical structure of the HBD on the conductive properties, morphological characteristics, and viscoelastic behavior of these mixed conducting eutectogels. Furthermore, we explored the suitability of the eutectogels for direct ink writing, creating different patterns. The printing geometry was correlated with the eutectogels impedances, obtaining good conformability for all the samples. Finally, the materials were placed on the skin, and the signal-to-noise ratio (SNR) was compared for the different geometries.

Results and discussion

To examine the effect of the DES chemical composition on the eutectogels properties, different HBD, such as –OH containing molecules glycerol and pyrogallol (GLY) and (PDO), natural organic acids such as lactic acid (LAC), and aromatic acids (PY and PTSA), were considered. The chemical structures of the eutectic mixture components are illustrated in Fig. 1(A). After the DES addition the PEDOT/PSS solution gelified and a supramolecular eutectogel consisted of the mixture of a DES with PEDOT:PSS in a specific ratio was formed Fig. 1(B). For explaining this, Muthukumar *et al.* found that PEDOT:PSS solutions are a dispersion of charged microgels that can connect by electrostatic interactions into a macroscopic network at moderate ionic strength in sufficiently high concentration.[26] Hence, if the concentration of PEDOT:PSS is lower than 30 wt%, the dilution effect and high ionic strength provided by the DES hamper the microgels crosslink. Conversely, if the PEDOT:PSS concentration exceeds 30 wt%, interactions achieve an equilibrium, forming a supramolecular eutectogel network (see Fig. 1(B)). We also observed phase segregation of the colloids if PEDOT:PSS concentration is over 60 wt%, probably due to ion-exchange processes. HBD may displace the PSS anion, unbalancing the charges of the supramolecular gel. FTIR analysis (Fig. S1A, ESI†) confirmed the characteristic signals of PEDOT:PSS at 1535 cm^{-1} (skeletal vibrations), 1254 cm^{-1} (RO–SO_3^- ν as), 1099 cm^{-1} (RO–SO_3^- ν sy), 1053 cm^{-1} (C–O–C ν), 950 cm^{-1} (C–H ν oop), and 660 cm^{-1} (C–S ν). After DES addition, signals attributed to the stretching vibrations of the sulfonic groups (SO_3H) in PSS[27]

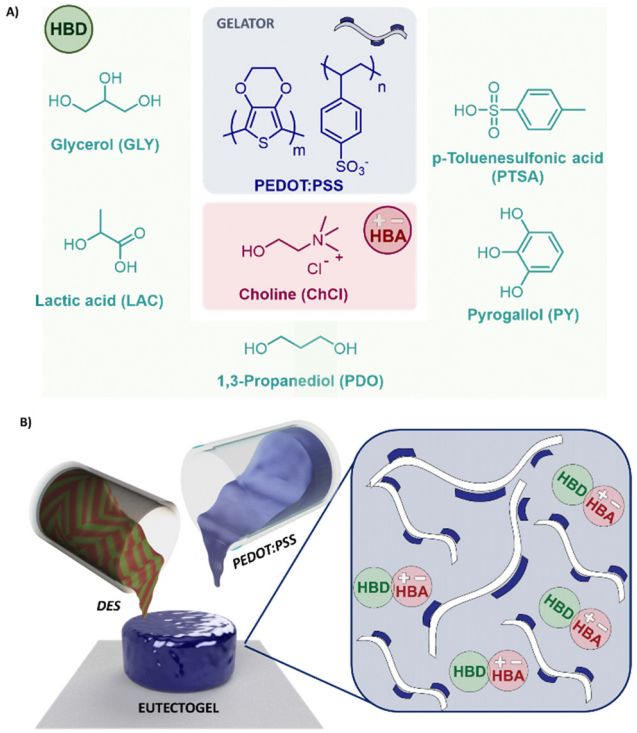

Fig. 1 (A) Chemical structures of PEDOT:PSS and DES used. (B) General pathway for preparing PEDOT:PSS/DES supramolecular eutectogels (left) and scheme of the interactions between the DES (HBA:HBD) and PEDOT:PSS when are mixed between 30 and 60 wt% (right).

displayed significant changes. For instance, Fig. S1B (ESI†) shows a red shift of the symmetric stretching vibration of SO_3^- from 1099 cm^{-1} to 1014 cm^{-1} for PEDOT:PSS/ChCl:LAC. Compared with the rest of the eutectogels, the electrostatic interaction of PSS with LAC indicates that the anion is effectively coupled to PEDOT displacing PSS. This effect has also been observed in PEDOT:PSS mixtures with cholinium lactate and imidazonium-based ILs.[15,28]

The intermolecular interactions of the supramolecular eutectogels could be decoded throughout their viscoelastic behavior monitoring the storage (G') and loss modulus (G'') at various strains.[29] Attractive electrostatic forces have the largest influence on stress-dependence properties as they require the most energy to disrupt, providing the greatest shear resistance.[30] Fig. S2A (ESI†) displays strain curves of all eutectogels *i.e.* 50/50 wt% PEDOT:PSS/DES. They all presented linear viscoelastic regime with constant values of G' and G'' up to 10% strain, followed by a sudden decay at 60% strain that point out the gel breakdown. This point indicates the disentanglement and rupture of the dynamic bonds, decreasing its forces and performing as fluid. In accordance, electron-rich DES *i.e.* ChCl:PTSA and ChCl:PY, present the largest storage modulus with 160 and 120 Pa, respectively. Therefore, we could assume π–π interactions between the styrene sulfonate of the PSS, the thiophene of PEDOT, and the benzyl moiety of the phenolic and tosylate DES. PEDOT:PSS composites with polyols ChCl:GLY and ChCl:PDO only possess the hydrogen bonding interactions, independently of the acceptor units (2 or 3 respectively), rendering an equal storage modulus of ≈70 Pa. Organic acid homologous, ChCl:LAC, does not present any additional impact on the intramolecular forces, decreasing to 40 Pa. In accordance, Fig. S2B (ESI†) shows the viscosity values of the eutectogels *vs.* frequency. The most viscous eutectogel is PEDOT:PSS/ChCl:PY with 1000 Pa s, being almost 10 times greater than the other mixtures, including the electron-riched PEDOT:PSS/ChCl:PTSA. Therefore, we could hypothesize that the combination of π–π interactions with hydrogen bonding of polyphenols plays a more remarkable role in the intermolecular forces than the combination of π-conjugated structures with sulfonated charges.

Besides the eutectogel formation, DES additives act as conductivity enhancements for PEDOT:PSS. Indeed, PEDOT:PSS/DES conductivity increased above two-three orders of magnitude compared with untreated PEDOT:PSS dispersion (~0.2 S cm^{-1}). The material conductivities were evaluated on a drop-casted deposition, measured in a semi-dry and dry state. We know from previous work performed with ionic liquids that the water content could enhance the conductivity of this mixed conducting material.[15] Firstly, the impact of the eutectogel composition was evaluated by a four-point probe on semi-wet films (see Fig. 2(A)). As expected, the conductivity is enhanced proportionally to the amount of DES added, reaching the maximum at 50/50 wt% (PEDOT:PSS/DES). After this composition, the conductivity drops consistently for all PEDOT:PSS/DES types, certainly due to the phase segregation effect. PEDOT:PSS/ChCl:PTSA displayed the highest conductivity for all compositions, 450 S cm^{-1}. It could be attributed to smoother inter-PEDOT-chain packing, also observed in vapor phase polymerization methods.[31] After PTSA, LAC is the most valuable HBD additive, improving conductivity up to 350 S cm^{-1}, especially for 50/50 wt% composition. Structurally comparative, lineal PDO enhanced 2.5-fold the conductivity than trifunctional GLY.

Fig. 2(B) and (C) shows the role of DES on the electronic and ionic conductivity deeply, the gel composition was fixed at 50/50 wt%, and both conductivities were evaluated in a dry state. It is known that high temperatures dry the film by lacking liquid solvent molecules and simplifying the system to a mixture of conducting polymer and dissolved ions.[32] Alcohols have been studied in detail in the literature as excellent solid polymer electrolytes leverage periodically repeating ether oxygen groups to coordinate and solvate cations. Therefore, PEDOT composites of ChCl:PDO and ChCl:PY are the ones that show the highest ionic conductivity values with 0.16 and 0.04 S cm^{-1} at 85 °C. (Fig. 2(C)) Also, these composites showed changes by a factor of two depending on temperature, demonstrating ionic-charges motion. On the opposite, composites with high electron-rich DES architectures presented lower values of ionic conductivities with 0.03 and 0.01 S cm^{-1} for ChCl:PY and ChCl:PTSA. Nyquist plots were evaluated to compare the ionic over the electronic contribution for each composition (see Fig. S3A–C, ESI†). These eutectogels present the more remarkable ionic conduction, independently of the temperature, characterized by a diffusive straight line. In contrast, composites with LAC and PTSA HBD presented mixed conduction at room temperature, besides the exclusive electronic-dominated mechanism observed by a semi-

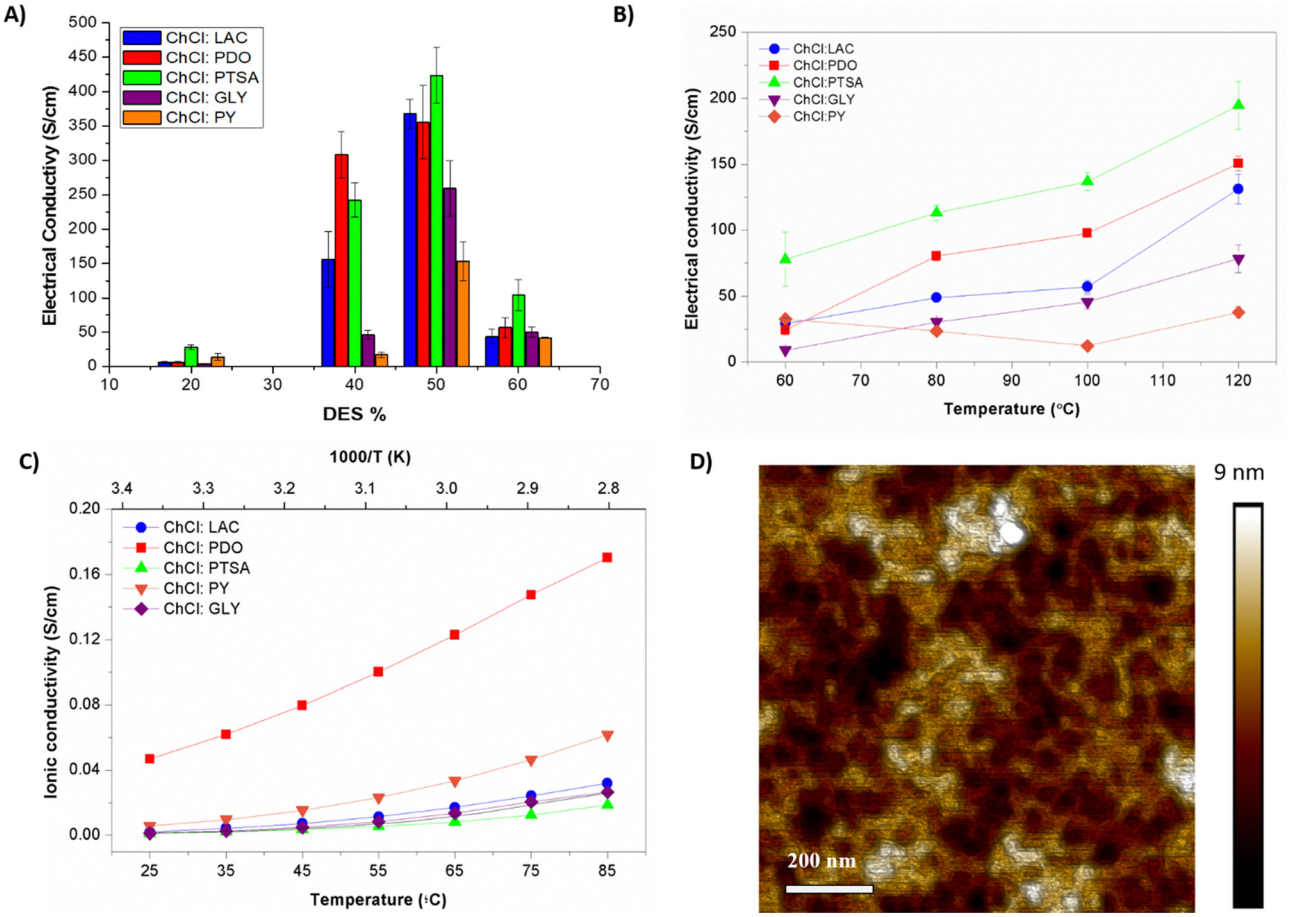

Fig. 2 (A) Electrical conductivities of PEDOT:PSS/DES composites with different DES amounts 20, 40, 50, and 60 wt%, (B) Electrical conductivities of 50/50 wt% PEDOT:PSS/DES composites measured by 4PP on dried films, (C) Ionic conductivities of 50 : 50 wt% PEDOT:PSS/DES calculated throughout fitting at different temperatures and (D) AFM height images of PEDOT:PSS/ChCl:LAC composite films annealed at 120 °C.

circle at high temperatures. This observation reveals that PEDOT:PSS/ChCl:PTSA, PEDOT:PSS/ChCl:PY, and PEDOT:PSS/ChCl:LAC composites are dominated by electronic conductivity mechanism while PEDOT:PSS/ChCl:PDO and PEDOT:PSS/ChCl:GLY eutectogels are dominated by ionic mechanisms.

Higher temperatures of annealing change structurally organic semiconductors, specially PEDOT:PSS.[33] In this regard, the electronic conductivity was evaluated at different annealing temperatures (Fig. 2(B)). The electronic conductivity revealed an enhancement by a factor of two for all the PEDOT:PSS/DES composites except for ChCl:PY films, which kept the conductivity constant at 50 S cm^{-1}. Fig. 2(D) shows the morphology of PEDOT:PSS/ChCl:LAC after 120 °C annealing. Dry eutectogels exhibited very uniform surfaces, indicating continuity throughout the film. The interconnection of the PEDOT-riched aggregates was originated from the significant phase separation between the PSS-rich shells and the PEDOT-rich cores. A high-performance DES should induce not only an efficient ion exchange with PEDOT:PSS to increase mobility but also a uniform high-level p-doping of PEDOT that increases its intrinsic conductivity.[34]

Supramolecular interactions in the PEDOT:PSS/DES eutectogels could be engineered to provoke reversible gel–sol transition, rendering them ideal materials for direct ink writing (DIW). Fig. 3(A) shows dynamic strain tests. At low strains (1%), the conducting composite behaves as a solid gel ($G' > G''$). After applying a high strain (1000%), G' drastically decreased, and the liquid-like state was reached ($G'' > G'$). Reversibly, when 1% strain is returned, the material recovers its initial moduli values without delay. DIW 3D printing was carried out using an extrusion-based printed commanded by aire pressure. The eutectogel was placed inside a plastic cartridge and extruded by 1–5 Pa compressed air. The action of pressure breaks the intramolecular interactions and confers its fluid-like state on the eutectogel. Subsequently, the material is printed in a desired shape and instantaneously recovered the gel-like consistency at room temperature (see Fig. 3(B)). In accordance with the viscosity test, electron-rich eutectogels present higher forces to perform the sol–gel transitions, which could cause clogging and impede its flow after the air-flow application. Meanwhile, the polyols and LAC present lower forces, being more friendly with this nozzle-dependent technique. Among the different eutectogels, PEDOT:PSS/ChCl:LAC was selected for further use due to its biocompatibility for skin contact and its suitable combination between mixed conductivity and rheological behavior. Moreover, PEDOT:PSS/ChCl:LAC eutectogels demonstrated retaining the electroactive behavior of the polymer after printing. Fig. S4 (ESI†)

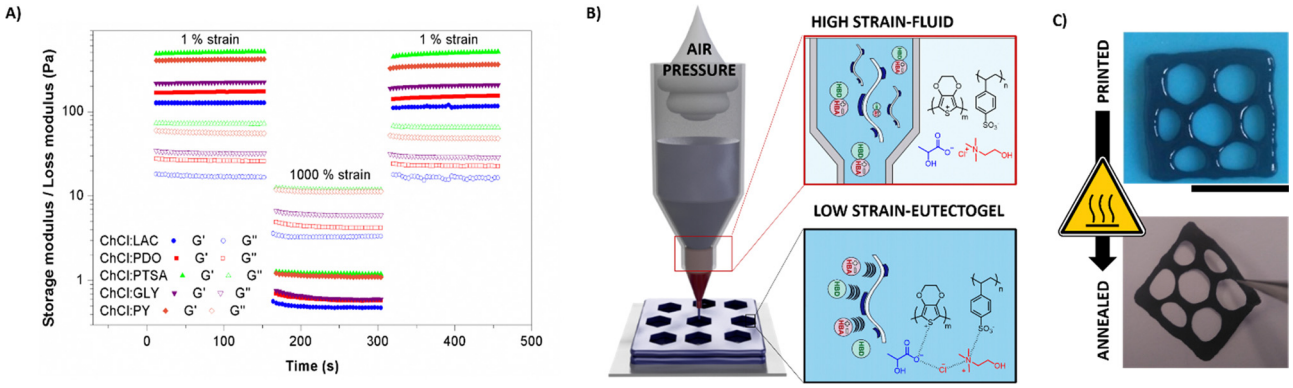

Fig. 3 (A) Dynamic strain tests alternating 1% and 1000% strain at short times of 500 s. (B) Scheme of the DIW method and changes in the interaction of the eutectogel strain function. (C) 3D printed hexagonal patterned PEDOT:PSS/ChCl:LAC eutectogel before and after the annealing process at 50 °C (scale bar = 1 cm).

shows the cyclic voltammetries (CVs) at different scan rates. The material showed a capacitive behavior with broad anodic and cathodic peaks at 0.4 V and 0.2 V *vs.* Ag/AgCl, typical of PEDOT-electroactive materials. Besides, the anodic and cathodic current increased proportionally with the scan rate, indicating that the redox process was not limited by diffusion and demonstrating that the whole eutectogel was involved in the electrochemical reaction. Fig. 3(C) shows the eutectogel DIW printed and its appearance when the material was annealed at 50 °C for 16 h until the water was removed. The final material is a ~20 μm thickness with self-portable capability and enough robustness to be peeled off and physically handled. Three different square shapes were printed with solid, hexagonal, and stripe patterns (see Fig. S5, ESI†). Squares areas were calculated using ImageJ processing (see Fig. S6, ESI†). DIW printed eutectogels presented areas of 2.0–2.3 cm^2 for the striped patterns, 2.3–2.5 cm^2 for the hexagonal patterns, and almost the double 3.9–4 cm^2 for the solid shapes. After printing, the dried pattern was connected with silver paste to a flexible cable and then adhered on top of a double-side adhesive-transfer paper.

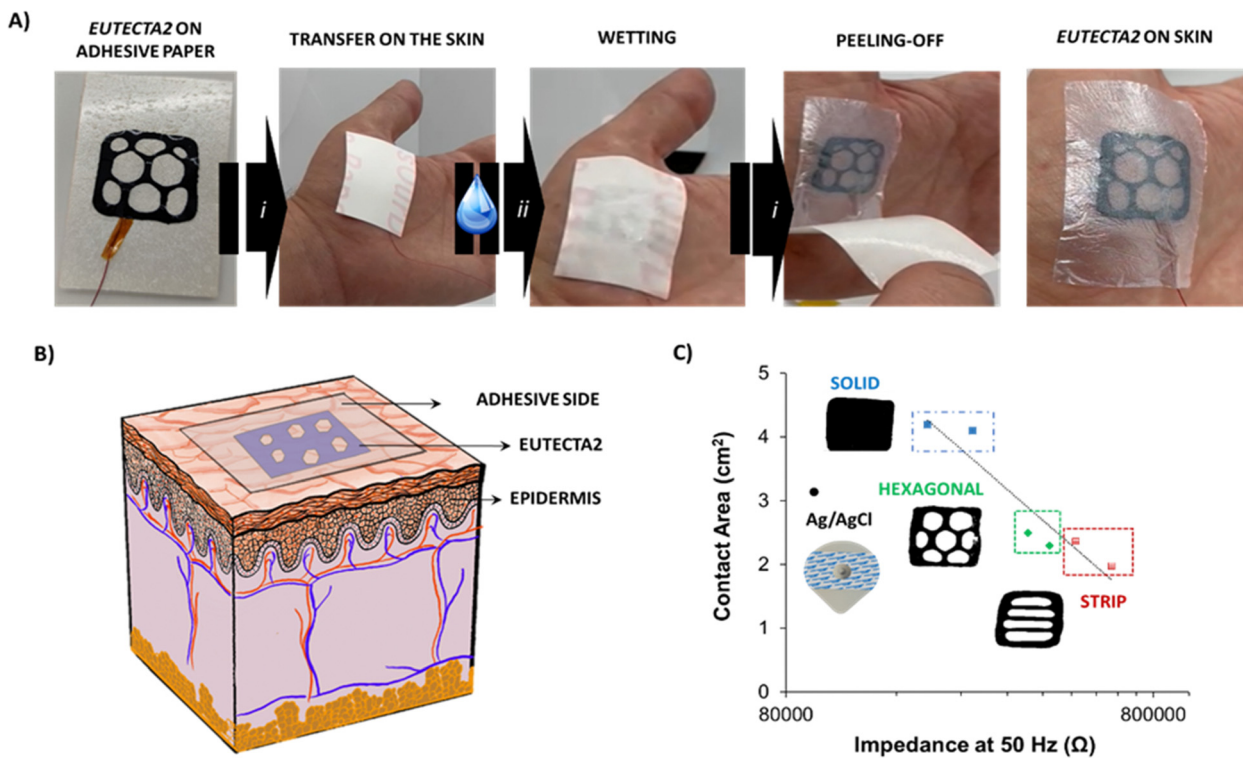

Fig. 4 (A) Schematic description of the sticker process, (i) Eutecta2 stuck on top of the skin, (ii) wetting step on the transfer paper side and (iii) peeled-off the transfer paper leaving the Eutecta2 in contact with the skin, (B) scheme of the Eutecta2 stuck on the skin for epidermal biopotential detections of electromyography (EMG) and (C) values of impedance at 50 Hz of the solid, hexagonal, stripped, and Ag/AgCl electrode *vs.* the contact area (Ag/AgCl contact area is 3.14 cm^2).[39]

Fig. S7 (ESI†) shows the final scheme of the geometry assembled, dubbed the Eutecta2. Fig. 4(A) shows the easily transferable mechanism on the skin, which consisted of three simple steps: (i) the Eutecta2 was placed on the skin with the help of the adhesive side paper and gentle pressure, (ii) a great amount of water was added to the surface, wetting the transfer paper and (iii) the transfer paper was peeled-off leaving the Eutecta2 in contact with the skin surface. Hereby, the Eutecta2 is stable, highly conductive, and conformable on the skin. Fig. 4(B) depicts the situation and conformability of the tattoo on the skin. The sticky side of the paper made it adhesive on the skin, enhancing the biopotential signal recording of muscle groups, *i.e.*, electromyography (EMG). EMG is a technique that records muscle activation and relaxation *vs.* signal amplitude depending on motion. It has been used to monitoring motion of vital sign, flexible wearables or glucose sensor, among other applications.[35–37] The most useful and important EMG frequencies range from 10 to 150 Hz.[38] EIS was investigated on the skin using two-electrode configuration. All the samples displayed a frequency-dependent response, showing high impedance values at lower frequencies. In addition, the range of impedances presented comparable order of magnitude to a commercial Ag/AgCl electrode (see Fig. S8, ESI†). For an equivalent comparison, the area influence of the Eutecta2 at 50 Hz was investigated. As expected, impedance values at 50 Hz were dependent on the total surface of the electrodes for the dry Eutecta2 (see Fig. 4(C)). The solid pattern showed the lower values of impedances (258 ± 56 kΩ), followed by the hexagonal pattern (364 ± 59 kΩ) and the stripped pattern (617 ± 120 kΩ). In comparison, wet Ag/AgCl electrodes show impedance values of 80 ± 32 kΩ. Impedance values of the Eutecta2 were in accordance with the areas of the electrodes measured, being the solid electrode the lowest, hexagonal the second and finally the striped pattern. Moreover, the surface morphology of the Eutecta2 was observed under scanning electron microscopy (SEM), pre- and after used onto the skin (Fig. S9, ESI†). After contact with the skin, a wrinkle-like surface could be observed on the Eutecta2 surface, showing similarities to epithelial-skin morphology. This effect remarks the highly intimate conformability of the tattoo on the skin if compared with the smoothness of the pristine material.

The EMG recordings were conducted by placing the electrodes as indicated in Fig. 5(A). For EMG, two motions were recorded: (i) forearm and (ii) thumb motion. All movements started from a resting position with the palm facing downward, and the forearm or thumb muscles were contracted four-five times, each over five seconds (Fig. 5(A)). The EMG recorded during both motions showed a distinctive signal response for all the geometries, as well as the commercial electrodes. The signal-to-noise (SNR) ratio was calculated by evaluating the ratio between the signal and the base voltages. In Fig. 5(B), forearm EMG motion is displayed. All the Eutecta2 showed lower values of SNR than commercial Ag/AgCl electrodes, being SNR equal to 1.8 ± 0.2 for stripped shapes, 2.0 ± 0.4 for solid shapes, 2.6 ± 0.8 for hexagonal shapes and 3.2 ± 1.5 for commercial Ag/AgCl. Surprisingly, the variable area of the electrode is not directly correlated with the EMG recording of the electrodes, indicating a conformability-dependent factor. The result indicates a compromise between contact area and impedance values to obtain ideal recordings. In order to corroborate our hypothesis, the EMG on thumb motion was

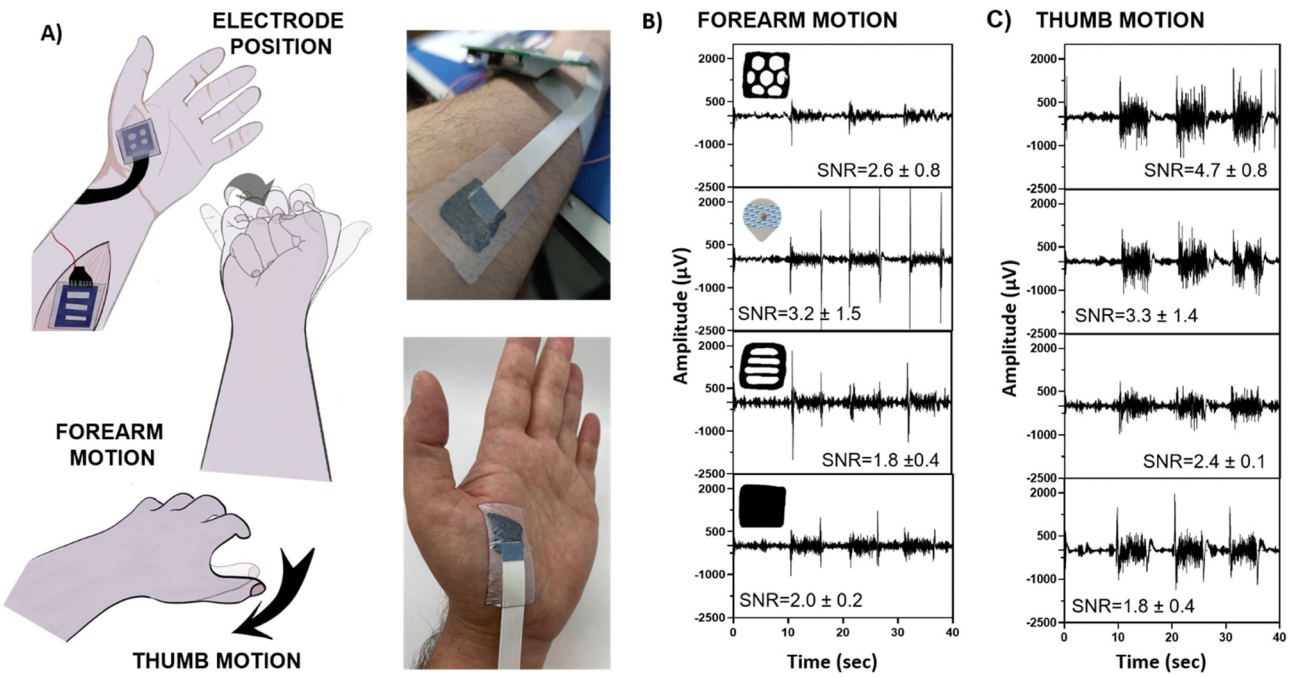

Fig. 5 (A) Schematic representation of the position of each electrode placed on the skin, indicating muscles involved in the movement (top), forearm (middle) and thumb motions (bottom). On the right, photos of the Eutecta2 placed on the skin are shown. EMG recordings on the forearm (B) and thumb (C) of hexagonal, striped, and solid Eutecta2, compared with Ag/AgCl electrodes. Signal-to-noise ratio (SNR) of each measurement is also shown.

recorded and displayed in Fig. 5(C). The location of the Eutecta2 on the thumb requires more adaptability of the electrode to the skin. In this case, hexagonal Eutecta2 showed the best performance with 4.7 ± 0.8 SNR values, followed by the commercial Ag/AgCl electrode with 3.3 ± 1.4, the stripped with 2.4 ± 0.1 and the solid electrode with 1.8 ± 0.4. All in all, we concluded that the Eutecta2 are conformable to muscles, allowing measurements in complex areas and therefore improving recording than commercially available electrodes.

Finally, the solid-shaped Eutecta2 was removed carefully, replaced 14 days later, and measured on the forearm, and its performance was compared with day 0. In contrast with many of the examples shown in the literature, the plasticity and self-portability of the electrodes and their high ionic–electronic conductivity allow for reusability after post-used. Fig. S10A (ESI†) shows the solid-shaped electrode after removal during day 0, demonstrating enough robustness. EMG recording after 14 days confirmed its reusability, displaying non-significant SNR values with 2.0 ± 0.4 for day 0 and 2.2 ± 0.2 for day 14 (see Fig. S10B, ESI†).

Experimental

Materials

All chemicals were used without any further purification. Choline chloride (ChCl, ≥98%, Sigma-Aldrich), 1,3 propanediol (PDO, 99%, Thermo Scientific™), glycerol (Gly, ReagentPlus®, ≥99.0%, Sigma-Aldrich), *p*-toluenesulfonic acid monohydrate (PTSA, ReagentPluss, ~98%, Sigma-Aldrich), DL-lactic acid (LAC, ~90%, Thermo Scientific™) and pyrogallol (PY, ≥98.0% HPLC, Sigma-Aldrich). Poly(3,4-ethylenedioxythiophene):poly(styrene sulfonate) (PH1000, Heraeus Clevios™).

Methods

DES synthesis. The DES were synthesized by the heating method, mixing ChCl and various HBD at 95 °C until a clear homogeneous liquid was obtained (except ChCl: lactic acid, where the temperature was set at 60 °C). The final obtained DES and their molar ratios were ChCl : LAC 1 : 2, ChCl : GLY 1 : 2, ChCl : PDO 1 : 2, ChCl : PTSA 1 : 1, and ChCl : PY 1 : 1.

Synthesis of the PEDOT:PSS/DES eutectogels. The corresponding amounts of Clevios™ and DES were mixed at room temperature with PEDOT:PSS/DES weight ratios of 80/20, 60/40, 50/50, and 40/60 (being the PEDOT:PSS amount calculated as 1.3% of the Clevios™ weight). Right after mixing, the PEDOT:PSS/DES composite was vortexed during ~30 seconds. When PEDOT:PSS/DES was mixed completely the viscosity of the composite was clearly increased with gel-like consistency. The gel-like material was poured on a silicon mould and then dried at 60 °C for 24 h, employing no vacuum. For further thermal treatments, gel-like composites were performed at 60, 80, 100, and 120 °C under vacuum for 1 h.

Electronic conductivity. The electronic conductivity of the dried samples was measured with a four-point probe Ossila system at room temperature. Three measurements were obtained; the average value among them is reported, with its corresponding deviation standard error.

Ionic conductivity. The ionic conductivity was measured by electrochemical impedance spectroscopy (EIS), employing an Autolab 302N potentiostat–galvanostat, coupled with a Microcell HC station, which provided temperature control. Both the DES and the dried composites were measured. DES were measured by being deposited inside a silicon mold of 8 mm intern diameter and approximately 1.245 mm thickness. The dried composite samples were 10 mm in diameter, previously vacuumed dried, and subjected to 1 h/120 °C thermal treatment. EIS measurements were carried out from 85 to 25 °C, with a step of 10 °C each, holding the temperature for 10 min and 20 min before each temperature change to allow temperature equilibrium in the whole sample. The frequency range was varied from 10^5 to 1 Hz, with 10 mV amplitude.

Cyclic voltammetry. Cyclic voltammetry measurements were performed in a three-electrode cell, employing a glassy carbon electrode (1 cm diameter) as the working electrode, an Ag/AgCl as the reference electrode, and a platinum as the counter electrode, in an aqueous NaCl 0.1 M solution as the electrolyte, and using a VMP3 potentiostat (Biological Science Instruments). The PEDOT:PSS/ChCl:LAC 50/50 liquid gel solution (5 μL) was drop-casted on the working electrode surface, dried at 60 °C under vacuum for 24 h, and then at 120 °C for 1 h. The system was purged with nitrogen for 10 min before measuring. The experiments were carried out at a potential range from −0.2 to 0.8 V (referenced to Ag/AgCl) at different scan rates (20, 50, 100, and 150 mV s^{-1}).

Fourier transform infrared spectroscopy (FTIR). FTIR was employed to characterize the structure of the dried composites, the DES, and the PEDOT:PSS. A Nicolet Magna 6700 spectrometer was used to acquire the spectra in the range of 400 to 4000 cm^{-1} with a 4 cm^{-1} resolution and averaged over 24 scans.

Rheological properties. The rheological behavior of the gels was analyzed with an AR-G2 rheometer (TA instruments) employing a cone-plate geometry. Storage and loss moduli were studied in dependence on three different variables: (i) strain oscillation (from 0.1 to 100% strain, at 1 Hz and 25 °C), temperature (from 0 to 90 °C, at 3% strain and 1 Hz), and angular frequency (from 0.1 to 100 rad s^{-1}, at 3% strain and 25 °C). Viscosity was studied as a function of temperature and shear rate. Shear rate measurements employed a rotational strain from 0.1 to 1000 s^{-1} at 25 °C, while temperature sweeps went from 25 to 90 °C at a rotation strain of 50 s^{-1}. Finally, injectability tests were implemented in time by performing a series of three steps of 150 s each, at 1 Hz: (i) at first, a strain of 1% was fixed; (ii) strain was raised to 1000%; (iii) finally, strain returned to its initial value of 1%.

3D direct ink writing (DIW) of Eutecta2. Printing tests were performed with a 3D-Bioplotter (Developer Series, EnvisionTEC, Gladbeck, Germany). The printed patterns were designed with the software Autodesk Inventor 2019. The printing process was performed at 25 °C, maximum pressure of 0.1 bar, 10 mm s^{-1} speed, and 0.001 mm of the maximum resolution. Needles with an inner diameter of 0.6 mm were used.

Eutecta2 preparation. For connection to the electronics, the Eutecta2 was first bonded to a cable using either silver paste or

medical tape. The silver paste was left to dry (40 °C after application) before undergoing thermal sintering (120 °C, 60 min) in a conventional oven, according to the manufacturer's specifications. Before placement on the skin, the tattoo was attached to a commercially available temporary tattoo sheet (TransOurDream, Glitter paper). The electrode was placed on the skin, applying hand pressure to ensure adhesion. The transfer paper was wetted using a DIW-soaked cloth that allows its removal, leaving the transparent one-side adhesive holding the electrode in intimate contact with the skin and protecting the Eutecta2.

***In vivo* recording.** All experimental EMG recording experiments were performed after approval of the Ethics Committee of the Department of Engineering at the University of Cambridge (6/9/2018, IONBIKE) and after obtaining informed consent from participants. The measurements were recorded using an RHS stimulation and recording system (Intan Technologies) at a 30 kHz sampling rate. Testing areas were gently wiped with a tissue wet in ethanol for skin preparation. Two different recording locations were selected for this paper, *i.e.* the inner forearm and hand thumb region. A commercial Ag/AgCl electrode (MLA 1010B, ADInstruments) was placed on the elbow for voltage reference. Recorded EMG signals were filtered using a 50 Hz band-stop filter and a band-pass filter with 10 Hz and 150 Hz cut-off frequencies. The signal-to-noise (SNR) ratio was calculated as the root mean squared (RMS) ratio of the measured voltage during muscular activation normalized by the number of samples, divided by the RMS of the signal measured when the forearm or the tumb was at rest, normalized as well by number of samples.

Conclusions

Overall, we have demonstrated the formation of supramolecular eutectogels combining PEDOT:PSS and several easy to prepare Deep Eutetic Solvents DES additives. The use of DES additives induces the gelification leading to the formation of conducting eutectogels. The resulting materials presented outstanding mixed ionic and electronic conductivity, time and air stability, as well as sol–gel reversibility. This property allowed direct ink writing in different designed shapes and patterns. After thermal annealing, flexible and skin-conformal dry mixed conductors could be obtained. In addition, we also showed a successful way to immobilize these novel Eutecta2 organic conductors on the skin to be used as e-tattoos. Finally, the e-tattoos were employed for EMG recording on non-conformable and conformable areas. The engineering of the material, combined with 3D printing and the e-tattoo transfer method, clearly offers super potential for future larger-area wearables, prosthetics, or implantable applications. Overall, these innovative mixed-conducting eutectogels could be promising alternatives to be implemented as conformable electrodes in bioelectronic devices for long-term health monitoring with high sensitivity.

Conflicts of interest

Authors confirms that there are no conflicts to declare.

Acknowledgements

This work was supported by Marie Sklodowska-Curie Research and Innovation Staff Exchanges (RISE) under grant agreement no. 823989 ''IONBIKE'' and AEI-MINECO for project PID2020-119026GB-I00. The financial support received from CONICET and ANPCyT (Argentina) is also gratefully acknowledged. Nerea Casado would like to thank the University of the Basque Country (no. 823989) for funding through a specialization of research staff fellowship (ESPDOC 19/99). Santiago Velasco-Bosom acknowledges the support from W. D. Armstrong Studentship. Antonio Dominguez-Alfaro acknowledges UPV/EHU for funding transferred by the European Union-Next Generation EU by the Margarita Salas fellowship (MARSA no. agreement 22/77). Eleni Mitoudi Vagourdi would like to acknowledge the Swedish Chemical Society.

Notes and references

1 S. S. Gambhir, T. J. Ge, O. Vermesh, R. Spitler and G. E. Gold, *Sci. Transl. Med.*, 2021, **15**(681), eabe5383.
2 L. Zhang, K. S. Kumar, H. He, C. J. Cai, X. He, H. Gao, S. Yue, C. Li, R. C. S. Seet, H. Ren and J. Ouyang, *Nat. Commun.*, 2020, **11**, 4683.
3 M. Berggren, E. D. Głowacki, D. T. Simon, E. Stavrinidou and K. Tybrandt, *Chem. Rev.*, 2022, **122**, 4826–4846.
4 G. Malliaras and I. McCulloch, *Chem. Rev.*, 2022, **122**, 4323–4324.
5 A. Spanu, M. Taki, G. Baldazzi, A. Mascia, P. Cosseddu, D. Pani and A. Bonfiglio, *Bioengineering*, 2022, **9**(5), 205.
6 G. Baldazzi, A. Spanu, A. Mascia, G. Viola, A. Bonfiglio, P. Cosseddu and D. Pani, *Computing in Cardiology (CinC)*, 2021, vol. 48, pp.1–4.
7 Y. Chen, G. Zhou, X. Yuan, C. Li, L. Liu and H. You, *Biosens. Bioelectron.*, 2022, **206**, 114118.
8 E. Bihar, T. Roberts, Y. Zhang, E. Ismailova, T. Hervé, G. G. Malliaras, J. B. De Graaf, S. Inal and M. Saadaoui, *Flexible Printed Electron.*, 2018, **3**, 034004.
9 A. Zucca, C. Cipriani, Sudha, S. Tarantino, D. Ricci, V. Mattoli and F. Greco, *Adv. Healthcare Mater.*, 2015, **4**, 983–990.
10 S. Taccola, A. Poliziani, D. Santonocito, A. Mondini, C. Denk, A. N. Ide, M. Oberparleiter, F. Greco and V. Mattoli, *Sensors*, 2021, **21**(4), 1197.
11 A. De Izarra, S. Park, J. Lee, Y. Lansac and Y. H. Jang, *J. Am. Chem. Soc.*, 2018, **140**(16), 5375–5384.
12 Y. Wang, C. Zhu, R. Pfattner, H. Yan, L. Jin, S. Chen, F. Molina-Lopez, F. Lissel, J. Liu, N. I. Rabiah, Z. Chen, J. W. Chung, C. Linder, M. F. Toney, B. Murmann and Z. Bao, *Sci. Adv.*, 2022, **3**, e1602076.
13 A. Romero, A. Santos, J. Tojo and A. Rodríguez, *J. Hazard. Mater.*, 2008, **151**(1), 268–273.
14 I. F. Mena, E. Diaz, J. Palomar, J. J. Rodriguez and A. F. Mohedano, *Chemosphere*, 2020, **240**, 124947.
15 N. Casado, S. Zendegi, L. C. Tomé, S. Velasco-Bosom, A. Aguzin, M. Picchio, M. Criado-Gonzalez, G. G. Malliaras, M. Forsyth and D. Mecerreyes, *J. Mater. Chem. C*, 2022, **10**, 15186–15193.
16 M. A. R. Martins, S. P. Pinho and J. A. P. Coutinho, *J. Solution Chem.*, 2019, **48**, 962–982.

17 M. L. Picchio, D. Minudri, D. Mantione, M. Criado-Gonzalez, G. Guzmán-González, R. Schmarsow, A. J. Müller, L. C. Tomé, R. J. Minari and D. Mecerreyes, *ACS Sustainable Chem. Eng.*, 2022, **10**(25), 8135–8142.
18 L. C. Tomé and D. Mecerreyes, *J. Phys. Chem. B*, 2020, **124**, 8465–8478.
19 Y. Liu, J. B. Friesen, J. B. McAlpine, D. C. Lankin, S. N. Chen and G. F. Pauli, *J. Nat. Prod.*, 2018, **81**, 679–690.
20 Y. Dai, J. van Spronsen, G. J. Witkamp, R. Verpoorte and Y. H. Choi, *Anal. Chim. Acta*, 2013, **766**, 61–68.
21 W. Wu, H. Zeng, W. Zhang, W. Zhang, H. Jiang, G. Wu, Z. Li, X. Wang, Y. Huang and Z. Lei, *J. Appl. Polym. Sci.*, 2022, 1–10.
22 Z. Zhu, C. Liu, Q. Jiang, H. Shi, J. Xu, F. Jiang, J. Xiong and E. Liu, *Synth. Met.*, 2015, **209**, 313–318.
23 Z. Zhu, C. Liu, H. Shi, Q. Jiang, J. Xu, F. Jiang, J. Xiong and E. Liu, *J. Polym. Sci., Part B: Polym. Phys.*, 2015, **53**, 885–892.
24 Y. Lu, R. Liu, X. C. Hang and D. J. Young, *Polym. Chem.*, 2021, **12**, 2115–2121.
25 M. L. Picchio, A. Gallastegui, N. Casado, N. Lopez-Larrea, B. Marchiori, I. del Agua, M. Criado-Gonzalez, D. Mantione, R. J. Minari and D. Mecerreyes, *Adv. Mater. Technol.*, 2022, **7**, 2101680.
26 M. A. Leaf and M. Muthukumar, *Macromolecules*, 2016, **49**(11), 4286–4294.
27 H. He, L. Zhang, X. Guan, H. Cheng, X. Liu, S. Yu, J. Wei and J. Ouyang, *ACS Appl. Mater. Interfaces*, 2019, **11**(29), 26185–26193.
28 A. L. Oechsle, J. E. Heger, N. Li, S. Yin, S. Bernstorff and P. Müller-Buschbaum, *Macromol. Rapid Commun.*, 2021, **42**, 2100397.
29 S. Samanta, S. Kim, T. Saito and A. P. Sokolov, *J. Phys. Chem. B*, 2021, **125**(33), 9389–9401.
30 R. Stefanovic, M. Ludwig, G. B. Webber, R. Atkin and A. J. Page, *Phys. Chem. Chem. Phys.*, 2017, **19**, 3297–3306.
31 D. R. Evans, *Chem. Commun.*, 2022, **58**, 4553–4560.
32 B. D. Paulsen, S. Fabiano and J. Rivnay, *Annu. Rev. Mater. Res.*, 2021, **51**(1), 73–99.
33 X. Wu, M. Stephen, T. C. Hidalgo, T. Salim, J. Surgailis, A. Surendran, X. Su, T. Li, S. Inal and W. L. Leong, *Adv. Funct. Mater.*, 2022, **32**, 2108510.
34 T. A. Yemata, Y. Zheng, A. K. K. Kyaw, X. Wang, J. Song, W. S. Chin and J. Xu, *Mater. Adv.*, 2020, **1**, 3233–3242.
35 J. Ouyang, *SmartMat*, 2021, **2**, 263–285.
36 Y. Khan, A. E. Ostfeld, C. M. Lochner, A. Pierre and A. C. Arias, *Adv. Mater.*, 2016, **28**, 4373–4395.
37 Q. Chen, Y. Zhao and Y. Liu, *Chin. Chem. Lett.*, 2021, **32**, 3705–3717.
38 S. J. K. O'Neill, Z. Huang, M. H. Ahmed, A. J. Boys, S. Velasco-Bosom, J. Li, R. M. Owens, J. A. McCune, G. G. Malliaras and O. A. Scherman, *Adv. Mater.*, 2022, **35**, 2207634.
39 S. Velasco-Bosom, N. Karam, A. Carnicer-Lombarte, J. Gurke, N. Casado, L. C. Tomé, D. Mecerreyes and G. G. Malliaras, *Adv. Healthcare Mater.*, 2021, **10**, 2100374.

